

Trotter24: A precision-guaranteed adaptive stepsize Trotterization for Hamiltonian simulations

Tatsuhiko N. Ikeda,^{1,2,*} Hideki Kono,^{3,1,†} and Keisuke Fujii^{4,5,1,6,‡}

¹*RIKEN Center for Quantum Computing, Wako, Saitama 351-0198, Japan*

²*Department of Physics, Boston University, Boston, Massachusetts 02215, USA*

³*Department of Applied Physics, The University of Tokyo, Hongo, Tokyo, 113-8656, Japan*

⁴*Graduate School of Engineering Science, Osaka University,*

1-3 Machikaneyama, Toyonaka, Osaka 560-8531, Japan.

⁵*Center for Quantum Information and Quantum Biology, Osaka University, 560-0043, Japan.*

⁶*Fujitsu Quantum Computing Joint Research Division at QIQB,*

Osaka University, 1-2 Machikaneyama, Toyonaka 560-0043, Japan

(Dated: November 16, 2023)

Choosing an optimal time step δt is crucial for an efficient Hamiltonian simulation based on Trotterization but difficult due to the complex structure of the Trotter error. Here we develop a method measuring the Trotter error without ancillary qubits by combining the second- and fourth-order Trotterizations rather than consulting with mathematical error bounds. Implementing this method, we construct an algorithm, which we name Trotter24, for adaptively using almost the largest stepsize δt , which keeps quantum circuits shallowest, within an error tolerance ϵ preset for our purpose. Trotter24 applies to generic Hamiltonians, including time-dependent ones, and can be generalized to any orders of Trotterization. Benchmarking it in a quantum spin chain, we find the adaptively chosen δt to be about ten times larger than that inferred from known upper bounds of Trotter errors. Trotter24 allows us to keep the quantum circuit thus shallower within the error tolerance in exchange for paying the cost of measurements.

I. INTRODUCTION

The rapid development of quantum devices in recent years has led researchers to find useful applications with significant quantum advantage [1–3]. On top of the eigenvalue problems [4–9], quantum many-body dynamics, or Hamiltonian simulation [10–15], is one of the most promising candidates because quantum computers could overcome the exponential complexity that classical computers face [5], enabling us to address intriguing dynamical phenomena like nonequilibrium phases of matter [16–19] and to implement fundamental quantum algorithms like phase estimation [20]. Among several algorithms for the Hamiltonian simulation, Trotterization [21, 22] is and will be used most commonly in the current noisy intermediate-scale quantum (NISQ [23]) era and the coming early fault-tolerant quantum computing (FTQC) era because it does not demand additional ancillary qubits or largely controlled quantum gates. Indeed, quantum advantage in Trotterized dynamics simulation has been reported using a 127-qubit NISQ computer only recently [24].

One major and presumably inevitable issue of Trotterization is the trade-off relation between the simulation accuracy and the circuit depth. The k -th order Trotterization accompanies an error of $O(\delta t^{k+1})$ during a single time step δt , which decreases when δt is taken shorter. In the meantime, the number of steps to reach a final time

increases, meaning a deeper quantum circuit. To suppress the gate depth, it is desirable to choose the largest possible stepsize δt , i.e., the shallowest circuit, within our error tolerance ϵ preset for our purposes.

However, it is difficult to find the optimal stepsize δt because the Trotter error is complex in generic many-body systems. According to the previous studies on the Trotter error, its upper bounds [25, 26] and typical values [27] are available. If we choose δt so that the upper bound is below our tolerance ϵ , the precision is guaranteed, but δt tends to be too small, as we will see below. On the other hand, if we choose δt based on the typical values, δt can be larger, but the precision guarantee is lost. Recently, Zhao et al. [28] proposed an approach where δt is chosen adaptively in each time step based on the energy expectation value and variance. Yet, the precision guarantee of this method is still elusive, and the applicability is limited to time-independent Hamiltonians [29].

In this paper, we propose a precision-guaranteed method for choosing almost the largest δt within a preset error tolerance ϵ , whose key concept is illustrated in Fig. 1. The stepsize δt is chosen based on the measurement of the actual error and, thereby, optimal to achieve our tolerance. The measurement of the Trotter error is executable on a quantum circuit, without knowing the exact solution, with the help of a higher-order Trotterization formula, like in the Runge-Kutta-Fehlberg (RKF) method for classical simulations. We mainly focus on the second-order Trotterization supplemented by the fourth-order formula, naming the method Trotter24 in analogy to RKF45. We benchmark Trotter24 in a quantum spin chain under time-independent and -dependent Hamilto-

* tatsuhiko.ikeda@riken.jp

† konofr0924@g.ecc.u-tokyo.ac.jp

‡ keisuke.fujii.ay@riken.jp

nians, finding that the adaptively chosen δt is about ten times larger than that inferred from the upper bound of Trotter errors.

II. MEASURING TROTTER ERROR IN EACH STEP

For simplicity, we first consider a time-independent Hamiltonian H consisting of two parts,

$$H = A + B, \quad (1)$$

where A and B do not necessarily commute with each other. Generalization to more noncommuting parts is straightforward, and we will generalize the arguments to time-dependent ones later in Sec. VI.

Before considering a sequence of time steps in later sections, we focus here on a single step and discuss how to measure the Trotter error. For this purpose, we assume that the quantum state at time t is known to be $|\psi(t)\rangle$ and consider evolving it by a small time step δt ,

$$|\psi(t + \delta t)\rangle = U(\delta t) |\psi(t)\rangle = e^{-iH\delta t} |\psi(t)\rangle. \quad (2)$$

Trotterization approximately decomposes $e^{-iH\delta t}$ into quantum-gate-friendly parts consisting of either A and B . Since the generalization to other formulas is straightforward, we focus, for concreteness, on the second-order formula $T_2(\delta t)$

$$T_2(\delta t) \equiv e^{-iA\delta t/2} e^{-iB\delta t} e^{-iA\delta t/2}, = e^{-iH\delta t + \Upsilon_3} \quad (3)$$

where $\Upsilon_3 = O(\delta t^3)$ is an anti-Hermitian error operator. These relations imply

$$|\psi_2(t + \delta t)\rangle \equiv T_2(\delta t) |\psi(t)\rangle = |\psi(t + \delta t)\rangle + O(\delta t^3), \quad (4)$$

meaning that $T_2(\delta t)$ approximates the exact one-step evolution within an error of $O(\delta t^3)$.

To quantify the error arising in the one step, we adopt the conventional fidelity error

$$\eta_F \equiv 1 - |\langle \psi(t + \delta t) | \psi_2(t + \delta t) \rangle|^2. \quad (5)$$

We can also use other quantities depending on our purposes and make parallel arguments. For example, when we are interested in the expectation value of an observable O , we care about the error in it,

$$\eta_O \equiv \langle \psi(t + \delta t) | O | \psi(t + \delta t) \rangle - \langle \psi_2(t + \delta t) | O | \psi_2(t + \delta t) \rangle. \quad (6)$$

In either case, calculating η_F or η_O is difficult because we do not know the exactly evolved state $|\psi(t + \delta t)\rangle$.

We remark that, although $|\psi_2(t + \delta t)\rangle$ involves an $O(\delta t^3)$ error, $\eta_F = O(\delta t^6)$, while $\eta_O = O(\delta t^3)$ holds as expected. This is because the leading $O(\delta t^3)$ term of $1 - \langle \psi(t + \delta t) | \psi_2(t + \delta t) \rangle$ is pure-imaginary as shown in

Appendix A, and its leading-order contribution of η_F is given by

$$\eta_F = \langle \psi(t) | (i\Upsilon_3)^2 | \psi(t) \rangle - \langle \psi(t) | (i\Upsilon_3) | \psi(t) \rangle^2 + O(\delta t^7), \quad (7)$$

where $i\Upsilon_3$ is Hermitian. Equation (7) dictates that η_F is the variance of the ‘‘observable’’ $i\Upsilon_3$, giving a way to estimate η_F using $|\psi(t)\rangle$ and the explicit form of $i\Upsilon_3$. Indeed this is a possible way of measuring η_F , but it requires, for generic many-body Hamiltonians, measuring numerous Hermitian operators involved in $i\Upsilon_3$ consisting of doubly nested commutators between A and B . Hence, in this work, we will focus on another way to estimate η_F and η_O with less sampling costs.

Our idea of estimating the errors is the following: In calculating η_F and η_O in the leading order, we can safely replace the exact $|\psi(t + \delta t)\rangle$ by a higher-order approximant. For instance, we utilize a fourth-order formula known as the Forest-Ruth-Suzuki (FRS) formula [30, 31], $T_4(\delta t)$ given by

$$\begin{aligned} T_4(\delta t) &\equiv e^{-i\frac{s}{2}A\delta t} e^{-isB\delta t} e^{-i\frac{1-2s}{2}A\delta t} e^{-i(1-2s)B\delta t} \\ &\quad \times e^{-i\frac{1-2s}{2}A\delta t} e^{-isB\delta t} e^{-i\frac{s}{2}A\delta t} \\ &= e^{-iH\delta t + \Upsilon_5}, \end{aligned} \quad (8)$$

$$(9)$$

where $s = (2 - 2^{1/3})^{-1}$ and $\Upsilon_5 = O(\delta t^5)$ is anti-Hermitian. These expressions lead to

$$|\psi_4(t + \delta t)\rangle \equiv T_4(\delta t) |\psi(t)\rangle = |\psi(t + \delta t)\rangle + O(\delta t^5), \quad (10)$$

meaning that $T_4(\delta t)$ approximates the exact evolution within an error of $O(\delta t^5)$, which is two-order more accurate than Eq. (4). We remark that the FRS formula is known to have a relatively larger error than other fourth-order formulas [32, 33] comprised of more exponentials, which could alternatively be used for $T_4(\delta t)$. Throughout this work, we adopt the FRS formula because it involves the minimum possible number of exponentials (i.e., the gate complexity), and we have not encountered any issues in our benchmark implementations below.

Replacing $|\psi(t + \delta t)\rangle$ by $|\psi_4(t + \delta t)\rangle$ in η_F and η_O , we obtain the following key analytical results (see Appendix A for derivation): For the fidelity error,

$$\eta_F = \eta_F^{(24)} + O(\delta t^8), \quad (11)$$

$$\eta_F^{(24)} \equiv 1 - |\langle \psi_4(t + \delta t) | \psi_2(t + \delta t) \rangle|^2, \quad (12)$$

and, for the observable error,

$$\eta_O = \eta_O^{(24)} + O(\delta t^5), \quad (13)$$

$$\begin{aligned} \eta_O^{(24)} &\equiv \langle \psi_4(t + \delta t) | O | \psi_4(t + \delta t) \rangle \\ &\quad - \langle \psi_2(t + \delta t) | O | \psi_2(t + \delta t) \rangle. \end{aligned} \quad (14)$$

Given that $\eta_F = O(\delta t^6)$ and $\eta_O = O(\delta t^3)$, these results mean that $\eta_F^{(24)}$ ($\eta_O^{(24)}$) coincides with η_F (η_O) in the

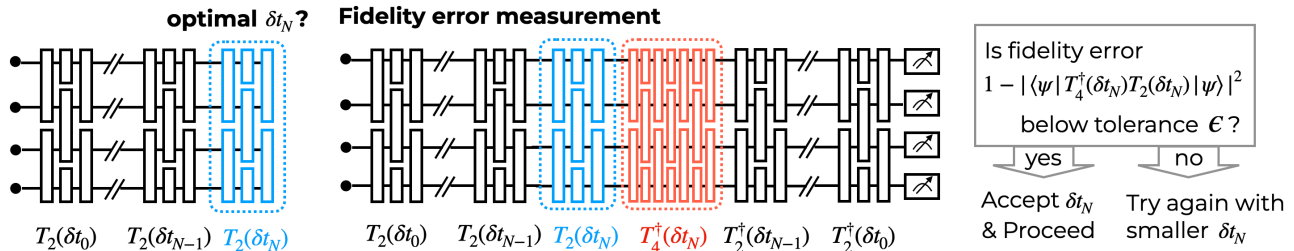


FIG. 1. Key concept of (fidelity-based) Trotter24. (Left) At each time step N , we ask what the optimal stepsize δt_N for the second-order Trotterization formula $T_2(\delta t_N)$. Here the optimal means the largest with the fidelity error kept less than our tolerance ϵ . (Middle) The fidelity error that $T_2(\delta t_N)$ can be measured using the fourth-order Trotterization $T_4(\delta t_N)$, instead of the exact evolution $U(\delta t_N)$ when we neglect higher-order corrections in terms of δt_N . (Right) If the measured error is below our tolerance, we accept the value of δt_N and proceed to the next time step $N + 1$. Otherwise, we reject the value and try the same protocol with a smaller value for δt_N again. In the paper, we also develop an observable-based, rather than fidelity-based, algorithm, establish an efficient scheme for avoiding the possible rejections of δt_N 's, and analyze how errors propagate with time steps.

leading order. Remarkably, unlike η_F and η_O , $\eta_F^{(24)}$ and $\eta_O^{(24)}$ consist of $T_2(\delta t)$ and $T_4(\delta t)$ and are thereby implementable in quantum circuits. In other words, we can estimate the deviation from the exact solution induced by $T_2(\delta t)$ without knowing the solution when supplemented with the fourth-order Trotterization and neglect higher-order corrections.

We emphasize that η_F and η_O are the actual Trotter error specific to the current state $|\psi(t)\rangle$. This contrasts the upper-bound arguments on the operator difference $U(\delta t) - T_2(\delta t)$ [25, 26]. Such upper bounds apply to arbitrary states and are thus always larger than or equal to the error occurring at a specific state $|\psi(t)\rangle$. The fact that η_F and η_O are state-dependent enables us to choose δt more accurately so that the error is below our tolerance, as we will see in detail below.

We remark on why we use the fourth-order rather than Ruth's third-order formula [22, 34],

$$T_3(\delta t) \equiv e^{-i\frac{7}{24}A\delta t} e^{-i\frac{2}{3}B\delta t} e^{-i\frac{3}{4}A\delta t} e^{i\frac{2}{3}B\delta t} \times e^{i\frac{1}{24}A\delta t} e^{-iB\delta t} \quad (15)$$

$$= e^{-iH\delta t + \Upsilon_4}, \quad (16)$$

where $\Upsilon_4 = O(\delta t^4)$. Replacing $T_4(\delta t)$ by $T_3(\delta t)$, one can easily make similar arguments to define $|\psi_3(t + \delta t)\rangle$, $\eta_F^{(23)}$, and $\eta_O^{(23)}$, proving that $\eta_F = \eta_F^{(23)} + O(\delta t^7)$ and $\eta_O = \eta_O^{(23)} + O(\delta t^4)$. Thus, $\eta_F^{(23)}$ ($\eta_O^{(23)}$) reproduces η_F (η_O) in the leading order and works as its estimator as well. Likewise, if we use an n -th ($n \geq 3$) order, we can have $\eta_F^{(2n)}$ ($\eta_O^{(2n)}$), which approximates η_F (η_O) in accuracy of $O(\delta t^{n+4})$ ($O(\delta t^{n+1})$). Meanwhile, using a larger n demands more exponentials (see Eqs. (8) and (15)), increasing the gate complexity. Nicely, $T_4(\delta t)$ has only one more exponential than $T_3(\delta t)$ in improving the accuracy by an order. Considering this reasonable balance between complexity and accuracy, we adopt $T_4(\delta t)$ for primary use.

III. ITERATION AND ENTIRE ALGORITHM

In the previous section, we assumed that $|\psi(t)\rangle$ is known and found error estimators $\eta_F^{(24)}$ and $\eta_O^{(24)}$ that consist of product formulas and hence implementable in quantum circuits. Here, we discuss how we choose an appropriate δt in successive steps of time evolution. As we see below, we can utilize the measured error estimator to determine a nearly optimal δt , thereby making the successive evolution efficient. Since the argument goes in parallel, we first focus on the fidelity error and will address the observable error later in this section.

Our overall task is to simulate the time evolution according to the Hamiltonian H from the initial time t_{ini} to the final time t_{fin} , starting from an initial state $|\psi_0\rangle$. We set an error tolerance ϵ for the fidelity error in each time step. Initially, we have no a priori information about the appropriate time step, so take a reasonably small trial stepsize δt_0 , say, $\delta t_0 = 0.1J^{-1}$ with J being a typical energy scale of H . One could also choose δt_0 so small that $T_2(\delta t_0)$ never gives larger error than our tolerance ϵ , as guaranteed by a mathematical bound (see Eq. (30) and Appendix C for detail). One can also use this δt_0 to know the upper bound, in advance, for the required quantum resources for the calculation, although they tend to be too pessimistic, as we will see below.

For the trial δt_0 taken in either way, we implement $T_2(\delta t_0)$ and $T_4(\delta t_0)$ and calculate $\eta_F^{(24)}$ using a quantum circuit. Basically, we aim the stepsize to be so small that

$$\eta_F^{(24)} < \epsilon. \quad (17)$$

If this is true, we accept our trial δt_0 and evolve our state as $|\psi_1\rangle = T_2(\delta t_0)|\psi_0\rangle$. If $\eta_F^{(24)} \geq \epsilon$ instead, our trial δt_0 is too large and we need a smaller $\delta t'_0$. In choosing $\delta t'_0$ appropriately, we invoke the leading-order scaling relation $\eta_F^{(24)} \approx \alpha \delta t_0^6$ for some unknown α independent of δt_0 . We can use this relation to estimate α by

$\alpha \approx \eta_F^{(24)}/\delta t_0^6$ since we measured $\eta_F^{(24)}$. For $\delta t'_0$, we expect $\eta_F^{(24)'} \approx \alpha(\delta t'_0)^6 \approx \eta_F^{(24)}(\delta t'_0/\delta t_0)^6$, which we wish is smaller than ϵ . Thus, the condition $\eta_F^{(24)'} < \epsilon$ leads to $\delta t'_0 \approx \delta t_0(\epsilon/\eta_F^{(24)})^{1/6}$ as an optimal choice within our error tolerance. For a safety margin, we introduce a constant C ($0 < C < 1$) and set $\delta t'_0 = C\delta t_0(\epsilon/\eta_F^{(24)})^{1/6}$ as an updated trial δt_0 . We repeat this update procedure until $\eta_F^{(24)}$ gets smaller than ϵ and accept the latest δt_0 to evolve our state as $|\psi_1\rangle = T_2(\delta t_0)|\psi_0\rangle$.

Next, we move on to the second step, using a time step δt_1 . In choosing this, we again use the latest $\eta_F^{(24)}$ obtained at the end of the previous time step. Since $|\psi_1\rangle \approx |\psi_0\rangle$, we can expect the error scaling coefficient α to be almost the same in the present and previous steps. Therefore, like in the updated trials within the previous time step, we have $\delta t_1 = C\delta t_0(\epsilon/\eta_F^{(24)})^{1/6}$ as a good candidate for the optimal stepsize in the present time step. We note that $\eta_F^{(24)}$ here is what was measured in the previous step, and we have not made any measurements in the present step yet. Using this δt_1 as a trial stepsize, we implement $T_2(\delta t_1)$ and $T_4(\delta t_1)$ and calculate $\eta_F^{(24)}$ using a quantum circuit. Depending on whether $\eta_F^{(24)}$ is less or greater than ϵ , we accept or update δt_1 like in the previous step.

The following iteration is straightforward and repeated until the accumulated evolution time $t_{\text{ini}} + \delta t_0 + \delta t_1 + \dots$ exceeds the final time t_{fin} . We summarize a pseudocode for the algorithm in Algorithm 1.

Algorithm1 Fidelity-based Trotter24

Input: Initial and final times, t_{ini} and t_{fin} , an initial state $|\psi_0\rangle$, a Hamiltonian $H = A + B$, an error tolerance ϵ , an initial stepsize δt_0 , a safety constant C ($0 < C < 1$), an oracle function FIDELITY($|\phi\rangle, |\psi\rangle$) that calculates $|\langle\phi|\psi\rangle|^2$.

Output: An ordered list of unitaries U_{list} that approximates $e^{-iH(t_{\text{fin}}-t_{\text{ini}})}$ within the error tolerance for each time step.

```

1:  $t \leftarrow t_{\text{ini}}$ 
2:  $\delta t \leftarrow \delta t_0$ 
3:  $U_{\text{list}} = \{\}$  (empty list)
4: while  $t + \delta t < t_{\text{fin}}$  do
5:    $|\psi(t)\rangle \leftarrow \prod_k (U_{\text{list}})_k |\psi_0\rangle$ 
6:   do
7:      $T_2(\delta t) \leftarrow e^{-iA\delta t/2} e^{-iB\delta t} e^{-iA\delta t/2}$ 
8:      $T_4(\delta t) \leftarrow e^{-i\frac{s}{2}A\delta t} e^{-isB\delta t} e^{-i\frac{1-s}{2}A\delta t} e^{-i(1-2s)B\delta t}$ 
      $\times e^{-i\frac{1-s}{2}A\delta t} e^{-isB\delta t} e^{-i\frac{s}{2}A\delta t}$ 
9:      $\eta \leftarrow 1 - \text{FIDELITY}(T_4(\delta t)|\psi(t)\rangle, T_2(\delta t)|\psi(t)\rangle)$ 
10:     $\delta t \leftarrow C \cdot (\epsilon/\eta)^{1/6} \delta t$ 
11:    while  $\eta > \epsilon$ 
12:    Prepend  $T_2(\delta t)$  to the ordered list  $U_{\text{list}}$ 
13:     $t \leftarrow t + \delta t$ 
return  $U_{\text{list}}$ 

```

Let us make a parallel argument for the observable error η_O instead of the fidelity error η_F . At each time step, we measure $\eta_O^{(24)}$ and judge if the condition

$$|\eta_O^{(24)}| < \epsilon_O \|O\| \quad (18)$$

is met. This is an analog of Eq. (17), and we introduced the operator norm $\|O\|$ as a reference scale and put the subscript O on the tolerance as ϵ_O to avoid confusion. The iteration scheme is parallel to the fidelity case, but the update of the stepsize comes with the exponent 1/3 instead of 1/6 since $\eta_O^{(24)} = O(\delta t^3)$ rather than $\eta_F^{(24)} = O(\delta t^6)$. We summarize a pseudocode for the observable-based algorithm in Algorithm 2.

Algorithm2 Observable-based Trotter24

Input: Initial and final times, t_{ini} and t_{fin} , an initial state $|\psi_0\rangle$, a Hamiltonian $H = A + B$, an error tolerance ϵ_O , an initial stepsize δt_0 , a safety constant C ($0 < C < 1$), an oracle function EXP($O, |\psi\rangle$) that calculates $\langle\psi|O|\psi\rangle$.

Output: An ordered list of unitaries U_{list} that approximates $e^{-iH(t_{\text{fin}}-t_{\text{ini}})}$ within the error tolerance for each time step.

```

1:  $t \leftarrow t_{\text{ini}}$ 
2:  $\delta t \leftarrow \delta t_0$ 
3:  $U_{\text{list}} = \{\}$  (empty list)
4: while  $t + \delta t < t_{\text{fin}}$  do
5:    $|\psi(t)\rangle \leftarrow \prod_k (U_{\text{list}})_k |\psi_0\rangle$ 
6:   do
7:      $T_2(\delta t) \leftarrow e^{-iA\delta t/2} e^{-iB\delta t} e^{-iA\delta t/2}$ 
8:      $|\psi_2\rangle \leftarrow T_2(\delta t)|\psi(t)\rangle$ 
9:      $T_4(\delta t) \leftarrow e^{-i\frac{s}{2}A\delta t} e^{-isB\delta t} e^{-i\frac{1-s}{2}A\delta t} e^{-i(1-2s)B\delta t}$ 
      $\times e^{-i\frac{1-s}{2}A\delta t} e^{-isB\delta t} e^{-i\frac{s}{2}A\delta t}$ 
10:     $|\psi_4\rangle \leftarrow T_4(\delta t)|\psi(t)\rangle$ 
11:     $\eta \leftarrow |\text{EXP}(O, |\psi_4\rangle) - \text{EXP}(O, |\psi_2\rangle)|$ 
12:     $\delta t \leftarrow C \cdot (\epsilon/\eta)^{1/3} \delta t$ 
13:    while  $|\eta| > \epsilon_O \|O\|$ 
14:    Prepend  $T_2(\delta t)$  to the ordered list  $U_{\text{list}}$ 
15:     $t \leftarrow t + \delta t$ 
return  $U_{\text{list}}$ 

```

IV. ERROR PROPAGATION

After N (≥ 1) steps, we obtain a quantum state

$$|\psi_2(t_N)\rangle = \prod_{i=0, \dots, N-1}^{\leftarrow} T_2(\delta t_i) |\psi_0\rangle \quad (19)$$

at time

$$t_N = t_{\text{ini}} + \sum_{i=0}^{N-1} \delta t_i \quad (20)$$

as an approximation for the exact state

$$|\psi(t_N)\rangle = \prod_{i=0, \dots, N-1}^{\leftarrow} U(\delta t_i) |\psi_0\rangle = e^{-iH(t_N-t_{\text{ini}})} |\psi_0\rangle. \quad (21)$$

This section gives upper bounds for accumulated errors in the N steps. As expected, we will have error propagation linear in N . Throughout this section, we let \sim and \lesssim denote $=$ and \leq , respectively, when sub-leading terms in δt_j ($j = 0, \dots, N-1$) are neglected.

For the fidelity-based Trotter24, let us find an upper bound for the accumulated error

$$\delta F_N \equiv 1 - |\langle \psi(t_N) | \psi_2(t_N) \rangle|^2. \quad (22)$$

As we derive in Appendix B,

$$\delta F_N \lesssim N^2 \epsilon, \quad (23)$$

meaning a quadratic increase in the fidelity error. This upper bound implies an upper bound for the error in the expectation value of an arbitrary observable O ,

$$\delta O_N \equiv |\langle \psi(t_N) | O | \psi(t_N) \rangle - \langle \psi_2(t_N) | O | \psi_2(t_N) \rangle|. \quad (24)$$

To derive the bound for δO_N , we recall $\delta O_N \leq 2D(|\psi(t_N)\rangle\langle\psi(t_N)|, |\psi_2(t_N)\rangle\langle\psi_2(t_N)|) \|O\|$, where $D(\rho, \sigma)$ denotes the trace distance, which is known to

satisfy $D(\rho, \sigma) \leq \sqrt{1 - F(\rho, \sigma)}$ with $F(\rho, \sigma)$ being the fidelity. Using Eq. (23), we obtain

$$\delta O_N \lesssim N \sqrt{\epsilon} \|O\|, \quad (25)$$

which linearly increases with N .

For the observable-based Trotter24 using an observable O , let us find an upper bound with the tolerance ϵ_O for the accumulated error (24) arising in the same observable. We can prove

$$\delta O_N \lesssim N \epsilon_O \|O\| \quad (26)$$

by induction on N . This claim trivially holds when $N = 1$ by the definition of δt_0 . Suppose that Eq. (26) for N . For $N + 1$, the triangle inequality gives

$$\begin{aligned} \delta O_{N+1} \leq & \left| \langle \psi(t_{N+1}) | O | \psi(t_{N+1}) \rangle - \langle \psi_2(t_N) | U^\dagger(\delta t_N) O U(\delta t_N) | \psi(t_N) \rangle \right| \\ & + \left| \langle \psi_2(t_N) | U^\dagger(\delta t_N) O U(\delta t_N) | \psi(t_N) \rangle - \langle \psi_2(t_{N+1}) | O | \psi_2(t_{N+1}) \rangle \right|. \end{aligned} \quad (27)$$

Since $U^\dagger(\delta t_N) O U(\delta t_N) \sim O$, the first term on the right-hand side is $\lesssim N \epsilon_O \|O\|$ by the inductive hypothesis. The second term on the right-hand side is less than $\epsilon_O \|O\|$, as implemented in the algorithm. Combining these two, we obtain $\delta O_{N+1} \lesssim (N + 1) \epsilon_O \|O\|$, which completes the induction.

V. BENCHMARK IMPLEMENTATION

Let us benchmark Trotter24 in a quantum spin chain, using a classical computer. First, we implement the fidelity-based Trotter24 and will address the observable-based one later in this section. Following Ref. [28], we consider the following Hamiltonian

$$A = h_x \sum_{i=1}^L \sigma_j^x, \quad B = \sum_{i=1}^L (J_z \sigma_j^z \sigma_{j+1}^z + h_z \sigma_j^z), \quad (28)$$

where σ_j^α are the Pauli matrices acting on the j -th site, periodic boundary conditions are imposed, and we set $J_z = -1.0$, $h_z = 0.2$, and $h_x = -2.0$. Taking the initial state fully polarized along the $-y$ direction, we let it evolve for a while. Figure 2(a) shows the expectation value of the x -magnetization density

$$m_x \equiv \frac{1}{L} \sum_{i=1}^L \sigma_j^x \quad (29)$$

for different tolerances $\epsilon = 10^{-3}$ and 10^{-4} at $L = 18$, and we set $C = 0.95$. As expected, for smaller tolerance, the simulated dynamics resemble the exact result

better, as shown in the upper panel. We note that we encounter few $\eta^{(24)} > \epsilon$ in these simulations; It happens three (five) times for $\epsilon = 10^{-3}$ (10^{-4}) during the simulation time range. These numbers further decrease as we decrease the safety constant C , as we will discuss below. Figure 2(b) shows the actual fidelity error η_F in those simulations. We confirm that the errors are well below the upper bound (23), especially in late times.

The adaptively chosen stepsize δt is significantly larger than the one obtained by the error-bound approach. According to Ref. [25], their tight error bound of the second-order product formula gives the possible maximum stepsize (see Appendix C for more detail)

$$\delta t_{\text{bound}} = \left(\frac{\epsilon}{\|[B, [B, A]]\| + \frac{1}{2} \|[A, [B, A]]\|} \right)^{1/3}, \quad (30)$$

for which the difference between $U(\delta t)$ and the second-order Trotterization does not exceed the tolerance ϵ . As shown in Fig. 2(c), the ratio of the adaptively chosen δt to δt_{bound} is roughly greater than 10. This means that the stepsize determined by the error bound tends to be too small for a given tolerance, and the adaptive stepsize is significantly larger. This discrepancy derives from the fact that Trotter24 utilizes the quantum state at each time step while the error bound applies to arbitrary states and tends to be too pessimistic.

The C -dependence of the algorithm is shown in Fig. 3. For various C ($0.8 \leq C \leq 1.0$), we run the Trotter24 with the other parameters being the same as in Fig. 2. Over the time interval $t_{\text{ini}} = 0.0$ and $t_{\text{fin}} = 2.0$, we measure the average of the adopted stepsize δt and the rejection

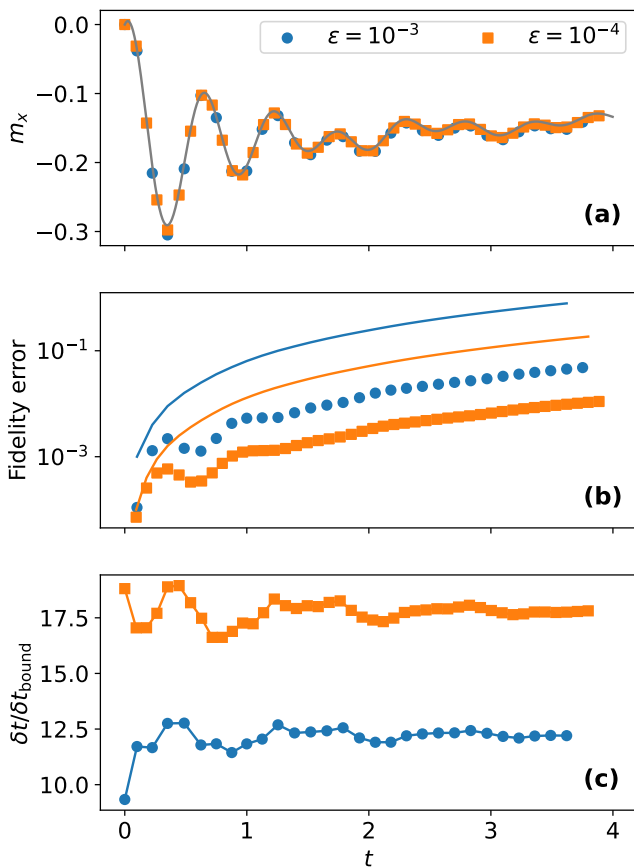


FIG. 2. (a) Dynamics of x -magnetization density calculated by fidelity-based Trotter24 for tolerance $\epsilon = 10^{-3}$ (circle) and 10^{-4} (square). The solid curve shows the accurate solution, the system size is $L = 18$, and the safety constant is $C = 0.95$. (b) The actual fidelity errors η_F (5) in the simulation presented in panel (a). The solid curves show their upper bounds (23). Blue (orange) points and curve correspond to the case of $\epsilon = 10^{-3}$ (10^{-4}). (c) The ratio of the stepsize δt chosen in each step to δt_{bound} obtained by the error-bound approach (30). Different symbols correspond to those in panel (a).

rate, i.e., the average number of occurrences of $\eta_F^{(24)} > \epsilon$ per each time step. As the left y -axis shows, the average stepsize is nearly proportional to C , as expected from its definition. Meanwhile, the rejection rate increases only slowly as C increases, except for the close vicinity of $C = 1$ ($0.99 \lesssim C \leq 1$), where C rapidly increases to exceed unity. If we never mind repeatedly measuring $\eta_F^{(24)}$, the choice $C = 1$ is ideal for making δt larger, i.e., the circuit depth shallower. However, by choosing a slightly smaller C , like $C = 0.95$ or 0.90 , we benefit from a dramatically-reduced rejection rate in exchange for a slight increase in the circuit depth.

Now we implement the observable-based Trotter24 for the same model (28) in the same setup. Suppose again that we are interested in simulating the dynamics of m_x . For this purpose, it is natural to set $O = m_x$, for which

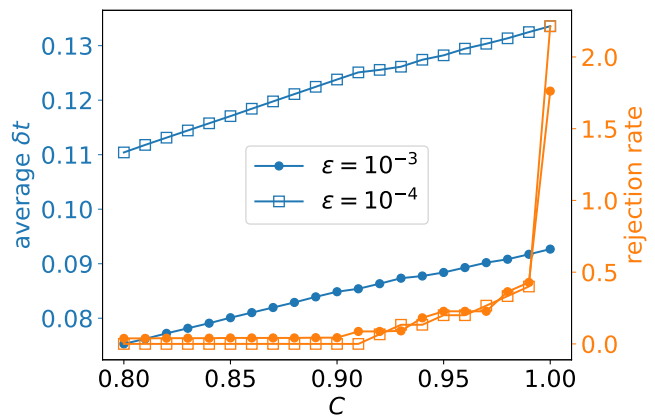


FIG. 3. The C -dependence of the average stepsize δt (left y -axis) and the rejection rate (right y -axis), i.e., the occurrence of $\eta_F^{(24)} > \epsilon$ per time step. Different symbols correspond to $\epsilon = 10^{-3}$ (circle) and 10^{-4} (square). The averages are taken for $t_{\text{ini}} = 0.0$ and $t_{\text{fin}} = 2.0$ with the initial trial stepsize $\delta t_0 = 0.1$.

the Trotter24 generates Fig. 4. For the smaller tolerance $\epsilon_O = 10^{-3}$, we obtain more accurate results for $\langle \psi(t) | m_x | \psi(t) \rangle$, as expected. As shown in panel (b), the stepsize is at least 5 times larger than δt_{bound} given by Eq. (30), whose values are $\delta t_{\text{bound}} = 2.31 \times 10^{-2}$ for $\epsilon = 10^{-2}$ and 1.07×10^{-2} for $\epsilon = 10^{-3}$. We note that the exact value always resides within the error bar representing the theoretical upper bound (26). Even when the exact values are not available, the upper bound tells us in what region they are.

Before closing this section, we remark on the stability and efficiency of Trotter24 for simulations over reasonably long times, as seen in Fig. 2(a). This is an advantage over extrapolation methods, such as Richardson's [35], in which physical quantities like $\langle \psi(t) | m_x | \psi(t) \rangle$ are obtained by extrapolating their estimates using different Trotter steps. The extrapolation methods are particularly useful for short times $t \ll 1$ (in units of an inverse local energy scale) because $\langle \psi(t) | m_x | \psi(t) \rangle$ is well approximated by a low-order polynomial in the Trotter steps and allows us to extrapolate the exact solution as the infinite steps limit [36]. For $t \gg 1$, however, the required steps increase significantly, and the estimates with limited steps tend to be unstable due to Runge's phenomenon (see Appendix D for demonstration). Although this pathologic behavior has been addressed using quantum singular value transformations [37], it requires a fault-tolerant quantum computer. When compared under the same gate complexity, Trotter24 is more stable than extrapolation methods, as detailed in Appendix D.

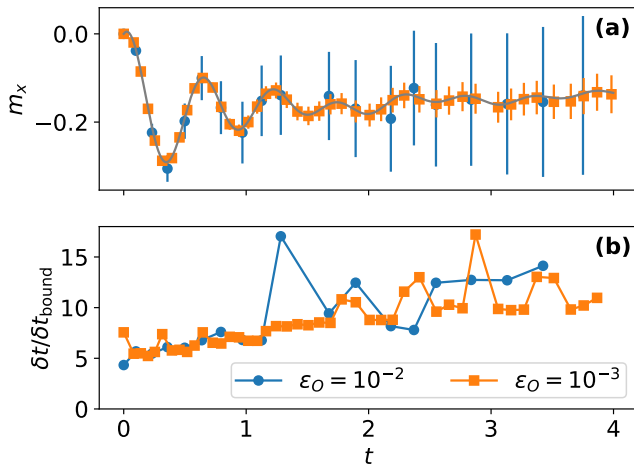


FIG. 4. (a) Dynamics of x -magnetization density m_x under the Hamiltonian (28) calculated by observable-based Trotter24 for $O = m_x$ and tolerance $\epsilon_O = 10^{-2}$ (circle) and 10^{-3} (square). The error bar shows the range where the exact solution resides as indicated by the theoretical upper bound (26). The solid curve shows an accurate solution obtained by a small enough δt , the system size is $L = 18$, and the safety constant is $C = 0.95$. (b) The ratio of the stepsize δt chosen in each step to δt_{bound} obtained by the error-bound approach (30) in the simulations shown in panel (a).

VI. GENERALIZATION TO TIME-DEPENDENT HAMILTONIANS

Trotter24, developed thus far for time-independent Hamiltonians, is straightforwardly generalized for time-dependent Hamiltonians unlike the previous study [28]. Their study is based on the energy conservation law, which is absent in time-dependent Hamiltonians, and its generalization to those Hamiltonians is not straightforward and has not been established yet.

Our setup is a generalization of Eq. (1) as

$$H(t) = A(t) + B(t), \quad (31)$$

and we consider approximating the exact evolution $|\psi(t)\rangle = U(t)|\psi_0\rangle$ for $U(t) = \mathcal{T} \exp\left(-i \int_0^t H(s) ds\right)$, where \mathcal{T} denotes the time ordering. Assuming that the quantum state $|\psi(t)\rangle$ at time t is known, we try to approximate the subsequent time evolution for a stepsize δt by the so-called midpoint rule

$$|\psi_2(t + \delta t)\rangle = T_2(t, \delta t) |\psi(t)\rangle, \quad (32)$$

$$T_2(t, \delta t) \equiv e^{-iA(t+\delta t/2)\frac{\delta t}{2}} e^{-iB(t+\delta t/2)\delta t} \times e^{-iA(t+\delta t/2)\frac{\delta t}{2}}. \quad (33)$$

The midpoint rule is known to be a second-order formula, and the fidelity error η_F and the observable error η_O are as small as $O(\delta t^6)$ and $O(\delta t^3)$, respectively, like in the time-independent-Hamiltonian cases.

To measure the errors in the leading order without using the exact state $|\psi(t + \delta t)\rangle$, we use a fourth-order Trotterization formula for time-dependent Hamiltonians. Focusing on a special case where $A(t) = a(t)A$ and $B(t) = b(t)B$ with $a(t)$ and $b(t)$ are scalars, we utilize the minimum fourth-order Trotterization formula [38]

$$|\psi_4(t + \delta t)\rangle = T_4(t, \delta t) |\psi(t)\rangle, \quad (34)$$

$$T_4(t, \delta t) \equiv e^{(\frac{s\beta_1}{2}-u)A} e^{s\beta_2 B} e^{\frac{1-s}{2}\beta_1 A} e^{(1-2s)\beta_2 B} \times e^{\frac{1-s}{2}\beta_1 A} e^{s\beta_2 B} e^{(\frac{s\beta_1}{2}+u)A} \quad (35)$$

consisting of seven exponentials, where $\beta_1 = \int_t^{t+\delta t} a(s) ds$, $\beta_2 = \int_t^{t+\delta t} b(s) ds$, and $\beta_{12} = \frac{1}{2} \int_t^{t+\delta t} dt_2 \int_t^{t_2} dt_1 [b(t_2)a(t_1) - a(t_2)b(t_1)]$, and $u \equiv \beta_{12}/\beta_2$ is assumed to be $O(\delta t^2)$. For more general $A(t)$ and $B(t)$, one can utilize the fourth-order Suzuki formula [22] consisting of 15 exponentials. We can define $\eta_F^{(24)}$ and $\eta_O^{(24)}$ similarly to the case of time-independent Hamiltonians and confirm that $\eta_F \approx \eta_F^{(24)}$ and $\eta_O \approx \eta_O^{(24)}$ in their leading orders.

The algorithms of Trotter24 for time-dependent Hamiltonians are obtained by the replacements $T_2(\delta t) \rightarrow T_2(t, \delta t)$ and $T_4(\delta t) \rightarrow T_4(t, \delta t)$ in Algorithms 1 and 2.

Let us now implement Trotter24 in an example time-dependent Hamiltonian. Our model is a generalization of Eq. (28) as

$$H(t) = tA + B, \quad (36)$$

where A and B are given in Eq. (28). We take the same initial state as in Sec. V and set the time interval as $t_{\text{ini}} = -3.0$ and $t_{\text{fin}} = +3.0$. Here we only demonstrate the observable-based one since the fidelity-based one works similarly. Figure 5 shows the x -magnetization density dynamics obtained by Trotter24 for different tolerance $\epsilon_O = 10^{-2}$ and 10^{-3} . Like in the time-independent case, Trotter24 provides the dynamics in a precision-guaranteed way, in which the exact solution resides in the error bars given by the preset tolerance ϵ_O .

Unlike in the time-independent case, the stepsize tends to decrease as $|t|$ increases, as shown in Fig. 5(b). This is consistent with the fact that the Hamiltonian (36), or the energy scale, is proportional to t when $|t| \gg 1$, for which the stepsize needs to be decreased to keep the error below the tolerance. Trotter24 automatically chooses the appropriate stepsize, depending on the instantaneous Hamiltonian as well as the instantaneous quantum state.

VII. CONCLUSIONS AND DISCUSSIONS

We have developed a method of measuring the Trotter error by combining it with another higher-order Trotterization without ancillary qubits. Using this, we devised an algorithm named Trotter24 for Hamiltonian simulations, during which the stepsize δt is adaptively chosen

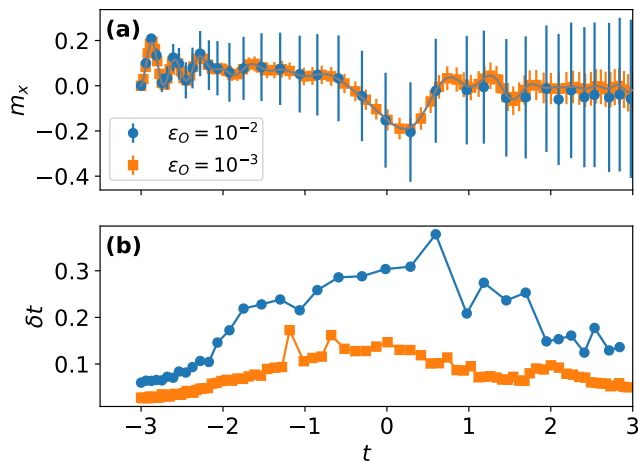


FIG. 5. (a) Dynamics of x -magnetization density, m_x , under the time-dependent Hamiltonian (36), calculated by observable-based Trotter24 for $O = m_x$ and tolerance $\epsilon_O = 10^{-2}$ (circle) and 10^{-3} (square). The error bar shows the theoretical upper bound (26). The solid curve shows an accurate solution obtained by the fourth-order Trotterization with $\delta t = 10^{-2}$, the system size is $L = 18$, and the safety constant is $C = 0.95$. (b) Stepsize δt chosen adaptively in the algorithm in each step. Different symbols correspond to those in panel (a).

as large as possible within an error tolerance we set in advance. In each time step, the precision is guaranteed in the sense of Eqs. (23) and (26) with higher-order corrections being neglected. Our algorithm applies to both time-independent and -dependent Hamiltonians, as we benchmarked in the example Hamiltonians in the quantum spin chain. Another merit of Trotter24 is the efficiency in finding the optimal stepsize δt . According to the benchmark, the estimated δt is rejected less than once on average during each time step by setting the safety constant $C \leq 0.99$. In exchange for conducting measurements in each step, Trotter24 adaptively finds almost the largest δt , which was about ten times as large as that inferred from the upper bound arguments. Thus, this algorithm keeps the circuit significantly shallower within our error tolerance ϵ .

Although we mainly discussed Trotter24, where the second-order Trotterization was supplemented with the fourth-order one, it is straightforward to generalize it to arbitrary order combinations to construct Trotter mn for $m < n$. As discussed in Sec. II, the second index n determines how accurate our error estimator $\eta_F^{(mn)}$ is. As n increases, with m held fixed, the estimator becomes more accurate, and so does the error guarantee. On the other hand, m determines the order of accuracy of the Trotterization; If we aim for super-accurate simulation like $\epsilon = 10^{-10}$, $m > 2$ would be more useful since the rapid decrease of error outweighs extra gate complexity in each step. Depending on the accuracy goals, one could choose an appropriate combination of m and n .

Although we focused on applying Trotter24 to quantum computers, this algorithm also applies to classical computations. Beyond the system sizes accessible with the full exact diagonalization of Hamiltonians, Trotterization-based algorithms, such as the time-evolution block-decimation [39] and the full state-vector evolution [8], are useful on high-performance computers. Trotter24 provides these classical computations with a precision-guaranteed adaptive stepsize method, enabling reliable simulations for quantum many-body dynamics.

We have neglected the statistical error in measuring the Trotter error through sampling and the device error inherent to NISQ computers. These errors are, in principle, estimated from the available number of measurements and the device assessment. Also, the error mitigation technique [35, 40] helps to reduce these errors, as demonstrated on a 100-qubit-scale NISQ computer [24]. If these errors are below our tolerance and the Trotter error is the bottleneck, Trotter24 will benefit us in optimizing Trotterization in a precision-guaranteed manner. We leave real-device implementations for future work.

ACKNOWLEDGEMENTS

Fruitful discussions with H. Zhao, J. Ostmeier, and K. Mizuta are gratefully acknowledged. T. N. I. is supported by JST PRESTO Grant No. JPMJPR2112 and by JSPS KAKENHI Grant No. JP21K13852. A part of numerical calculations has been performed using Qulacs [41]. This work is supported by MEXT Quantum Leap Flagship Program (MEXTQLEAP) Grant No. JPMXS0118067394, JPMXS0120319794, and JST COINEX program Grant No. JPMJPF2014.

Appendix A: Error Properties of Trotter24

1. Leading-order expression for η_F

According to the BCH formula, we have

$$U(\delta t)^\dagger T_2(\delta t) = e^{iH\delta t} e^{-iH\delta t + \Upsilon_3} = e^{\tilde{\Upsilon}_3}, \quad (\text{A1})$$

where

$$\tilde{\Upsilon}_3 = \Upsilon_3 + [iH\delta t, \Upsilon_3] + \dots = \Upsilon_3 + O(\delta t^4) \quad (\text{A2})$$

is an anti-Hermitian operator, and we used $\Upsilon_3 = O(\delta t^3)$. Thus, we have

$$|\langle \psi(t + \delta t) | \psi_2(t + \delta t) \rangle|^2 = |\langle \psi(t) | e^{\tilde{\Upsilon}_3} | \psi(t) \rangle|^2 \quad (\text{A3})$$

$$= |\langle \psi(t) | \left[1 + \tilde{\Upsilon}_3 + \frac{1}{2} \tilde{\Upsilon}_3^2 + O(\delta t^9) \right] | \psi(t) \rangle|^2 \quad (\text{A4})$$

$$= 1 + \langle \psi(t) | \tilde{\Upsilon}_3^2 | \psi(t) \rangle + |\langle \psi(t) | \tilde{\Upsilon}_3 | \psi(t) \rangle|^2 + O(\delta t^9) \quad (\text{A5})$$

$$= 1 - \langle \psi(t) | (i\tilde{\Upsilon}_3)^2 | \psi(t) \rangle + \langle \psi(t) | (i\tilde{\Upsilon}_3) | \psi(t) \rangle^2 + O(\delta t^9) \quad (\text{A6})$$

$$= 1 - \langle \psi(t) | (i\Upsilon_3)^2 | \psi(t) \rangle + \langle \psi(t) | (i\Upsilon_3) | \psi(t) \rangle^2 + O(\delta t^7), \quad (\text{A7})$$

where we used $\text{Re} \langle \psi(t) | \tilde{\Upsilon}_3 | \psi(t) \rangle = 0$ (since $\tilde{\Upsilon}_3$ is anti-Hermitian) and Eq. (A2). Therefore, we obtain

$$\eta_F = \langle \psi(t) | (i\Upsilon_3)^2 | \psi(t) \rangle - \langle \psi(t) | (i\Upsilon_3) | \psi(t) \rangle^2 + O(\delta t^7). \quad (\text{A8})$$

Notice that the right-hand side is nonnegative since $i\Upsilon_3$ is Hermitian.

2. Fidelity difference between the exact and fourth-order expressions

Here we study the difference between

$$\chi \equiv \langle \psi(t + \delta t) | \psi_2(t + dt) \rangle, \quad (\text{A9})$$

$$\chi_{24} \equiv \langle \psi_4(t + \delta t) | \psi_2(t + dt) \rangle \quad (\text{A10})$$

and show $\eta_F = 1 - |\chi_{24}|^2 + O(\delta t^8)$. We begin by noting

$$\chi - \chi_{24} = \langle \psi(t) | U^\dagger(\delta t) [1 - U(\delta t) T_4^\dagger(\delta t)] T_2(\delta t) | \psi(t) \rangle. \quad (\text{A11})$$

According to the BCH formula, we have

$$U(\delta t)^\dagger T_4(\delta t) = e^{iH\delta t} e^{-iH\delta t + \Upsilon_5} = e^{\tilde{\Upsilon}_5}, \quad (\text{A12})$$

where

$$\tilde{\Upsilon}_5 = \Upsilon_5 + [iH\delta t, \Upsilon_5] + \dots = O(\delta t^5) \quad (\text{A13})$$

is an anti-Hermitian operator, and we used $\Upsilon_5 = O(\delta t^5)$. Thus we have

$$\chi - \chi_{24} = \langle \psi(t) | U^\dagger(\delta t) \tilde{\Upsilon}_5 T_2(\delta t) | \psi(t) \rangle + O(\delta t^{10}) \quad (\text{A14})$$

$$= \langle \psi(t) | T_2^\dagger(\delta t) \tilde{\Upsilon}_5 T_2(\delta t) | \psi(t) \rangle + O(\delta t^8), \quad (\text{A15})$$

where we used $U(\delta t) = T_2(\delta t) + O(\delta t^3)$ and $\tilde{\Upsilon}_5 = O(\delta t^5)$. Since $\tilde{\Upsilon}_5$ is anti-Hermitian,

$$\delta\chi \equiv \langle \psi(t) | T_2^\dagger(\delta t) \tilde{\Upsilon}_5 T_2(\delta t) | \psi(t) \rangle = O(\delta t^5) \quad (\text{A16})$$

is pure imaginary.

Now we rewrite η_F using χ_{24} as follows,

$$\eta_F = 1 - |\chi|^2 = 1 - |\chi_{24} + \delta\chi|^2 \quad (\text{A17})$$

$$= 1 - |\chi_{24}|^2 - (\chi_{24}^* \delta\chi + \text{c.c.}) + O(\delta t^{10}). \quad (\text{A18})$$

Here we note

$$\chi_{24} = \langle \psi(t) | T_4(\delta t)^\dagger T_2(\delta t) | \psi(t) \rangle \quad (\text{A19})$$

$$= \langle \psi(t) | [T_4(\delta t)^\dagger U(\delta t)] [U^\dagger(\delta t) T_2(\delta t)] | \psi(t) \rangle \quad (\text{A20})$$

$$= \langle \psi(t) | e^{-\tilde{\Upsilon}_5} e^{\tilde{\Upsilon}_3} | \psi(t) \rangle \quad (\text{A21})$$

$$= 1 + \langle \psi(t) | \tilde{\Upsilon}_3 | \psi(t) \rangle + O(\delta t^5) \quad (\text{A22})$$

where we used Eqs. (A1) and (A12) to have Eq. (A21), and Eq. (A13) to obtain Eq. (A22). Substituting Eq. (A22) and using the facts $\text{Re} \delta\chi = 0$, $\delta\chi = O(\delta t^5)$, and $\tilde{\Upsilon}_3 = O(\delta t^3)$, we obtain

$$\eta_F = 1 - |\chi_{24}|^2 + O(\delta t^8). \quad (\text{A23})$$

3. Observable difference between the exact and fourth-order expressions

Here we show

$$\eta_O - \eta_O^{(24)} = O(\delta t^5). \quad (\text{A24})$$

This is simply obtained from

$$\langle \psi_4(t + \delta t) | O | \psi_4(t + \delta t) \rangle = \langle \psi(t) | e^{iH\delta t - \Upsilon_5} O e^{-iH\delta t + \Upsilon_5} | \psi(t) \rangle \quad (\text{A25})$$

$$= \langle \psi(t) | e^{iH\delta t} e^{-\Upsilon_5} O e^{\Upsilon_5} e^{-iH\delta t} | \psi(t) \rangle + O(\delta t^6) \quad (\text{A26})$$

$$= \langle \psi(t + \delta t) | O | \psi(t + \delta t) \rangle - \langle \psi(t) | [\Upsilon_5, O] | \psi(t) \rangle + O(\delta t^6) \quad (\text{A27})$$

$$= \langle \psi(t + \delta t) | O | \psi(t + \delta t) \rangle + O(\delta t^5), \quad (\text{A28})$$

which means

$$\begin{aligned} \eta_O - \eta_O^{(24)} &= \langle \psi(t + \delta t) | O | \psi(t + \delta t) \rangle - \langle \psi_4(t + \delta t) | O | \psi_4(t + \delta t) \rangle \\ &= O(\delta t^5). \end{aligned} \quad (\text{A29})$$

Appendix B: Fidelity Error Propagation

To prove Eq. (23), we begin by introducing

$$\delta U(\delta t) \equiv T_2^\dagger(\delta t) U(\delta t) - 1 = e^{-\tilde{\Upsilon}_3(\delta t)} - 1 = O(\delta t^3), \quad (\text{B1})$$

where we used Eq. (A2) and explicitly showed the δt -dependence of $\tilde{\Upsilon}_3$. Introducing

$$\Gamma_3(\delta t) \equiv i\tilde{\Upsilon}_3(\delta t) = O(\delta t^3), \quad (\text{B2})$$

which is Hermitian, we have

$$\delta U(\delta t) = e^{i\Gamma_3(\delta t)} - 1 = i\Gamma_3(\delta t) - \frac{\Gamma_3(\delta t)^2}{2} + O(\delta t^9). \quad (\text{B3})$$

Now we define

$$\chi_N \equiv \langle \psi(t_N) | \psi_2(t_N) \rangle, \quad (\text{B4})$$

which satisfies

$$\delta F_N = 1 - |\chi_N|^2. \quad (\text{B5})$$

Then we have

$$\chi_N = \langle \psi_0 | \prod_{i=0, \dots, N-1}^{\rightarrow} \left\{ T_2^\dagger(\delta t) \left[1 + i\Gamma_3(\delta t_i) - \frac{\Gamma_3(\delta t_i)^2}{2} \right] \right\} \prod_{i=0, \dots, N-1}^{\leftarrow} T_2(\delta t_i) | \psi_0 \rangle \quad (\text{B6})$$

$$\begin{aligned} &= 1 - i \sum_{i=1}^N \langle \psi(t_i) | \Gamma_3(\delta t_i) | \psi(t_i) \rangle - \frac{1}{2} \sum_{i=1}^N \langle \psi(t_i) | \Gamma_3(\delta t_i)^2 | \psi(t_i) \rangle \\ &\quad - \sum_{1 \leq i < j \leq N} \langle \psi(t_i) | \Gamma_3(\delta t_i) T_2^\dagger(\delta t_{i+1}) \cdots T_2^\dagger(\delta t_j) \Gamma_3(\delta t_j) | \psi(t_j) \rangle + O(\delta t^9); \end{aligned} \quad (\text{B7})$$

$$\begin{aligned} \delta F_N &= \sum_{i=1}^N \langle \psi(t_i) | \Gamma_3(\delta t_i)^2 | \psi(t_i) \rangle + 2\text{Re} \left[\sum_{1 \leq i < j \leq N} \langle \psi(t_i) | \Gamma_3(\delta t_i) T_2^\dagger(\delta t_{i+1}) \cdots T_2^\dagger(\delta t_j) \Gamma_3(\delta t_j) | \psi(t_j) \rangle \right] \\ &\quad - \left(\sum_{i=1}^N \langle \psi(t_i) | \Gamma_3(\delta t_i) | \psi(t_i) \rangle \right)^2 + O(\delta t^9), \end{aligned} \quad (\text{B8})$$

where we used $\text{Im} \langle \psi(t_i) | \Gamma_3(\delta t_i) | \psi(t_i) \rangle = 0$. Here we no-

tice that

$$\begin{aligned} &\|T_2(\delta t_j) \cdots T_2(\delta t_i) \Gamma_3(\delta t_i) | \psi(t_i) \rangle - \Gamma_3(\delta t_j) | \psi(t_j) \rangle\|^2 \\ &= \langle \psi(t_i) | \Gamma_3(\delta t_i)^2 | \psi(t_i) \rangle + \langle \psi(t_j) | \Gamma_3(\delta t_j)^2 | \psi(t_j) \rangle - 2\text{Re}[\langle \psi(t_i) | \Gamma_3(\delta t_i) T_2^\dagger(\delta t_{i+1}) \cdots T_2^\dagger(\delta t_j) \Gamma_3(\delta t_j) | \psi(t_j) \rangle] \end{aligned} \quad (\text{B9})$$

is higher-order and negligible in our leading-order calculations, meaning that we can replace $2\text{Re}[\langle \psi(t_i) | \Gamma_3(\delta t_i) T_2^\dagger(\delta t_{i+1}) \cdots T_2^\dagger(\delta t_j) \Gamma_3(\delta t_j) | \psi(t_j) \rangle]$ by $\langle \psi(t_i) | \Gamma_3(\delta t_i)^2 | \psi(t_i) \rangle + \langle \psi(t_j) | \Gamma_3(\delta t_j)^2 | \psi(t_j) \rangle$ neglecting higher-order corrections. By doing so and completing squares, we obtain

$$\begin{aligned} \delta F_N &\approx N \sum_{i=1}^N [\langle \psi(t_i) | \Gamma_3(\delta t_i)^2 | \psi(t_i) \rangle - \langle \psi(t_i) | \Gamma_3(\delta t_i) | \psi(t_i) \rangle^2] \\ &\quad + \sum_{1 \leq i < j \leq N} (\langle \psi(t_i) | \Gamma_3(\delta t_i) | \psi(t_i) \rangle - \langle \psi(t_j) | \Gamma_3(\delta t_j) | \psi(t_j) \rangle)^2 \end{aligned} \quad (\text{B10})$$

We notice again that the second term on the right-hand side of Eq. (B10) is negligible in the leading-order calculation. Recalling Eq. (7), we notice that the first term consists of the leading-order fidelity error in each time

step, which is guaranteed to be less than ϵ in the algorithm. Therefore we finally obtain

$$\delta F_N \lesssim N^2 \epsilon. \quad (\text{B11})$$

Appendix C: Error-bound approach

Here we apply the exact error bound [25] for our example model, obtaining δt guaranteeing the error is less than our tolerance ϵ . According to Ref. [25], we have the following inequality

$$\|U(\delta t) - e^{-iA\delta t/2} e^{-iB\delta t} e^{-iA\delta t/2}\| \leq W_{A,B} \delta t^3, \quad (\text{C1})$$

where

$$W_{A,B} \equiv \|[B, [B, A]]\| + \frac{1}{2} \|[A, [B, A]]\|. \quad (\text{C2})$$

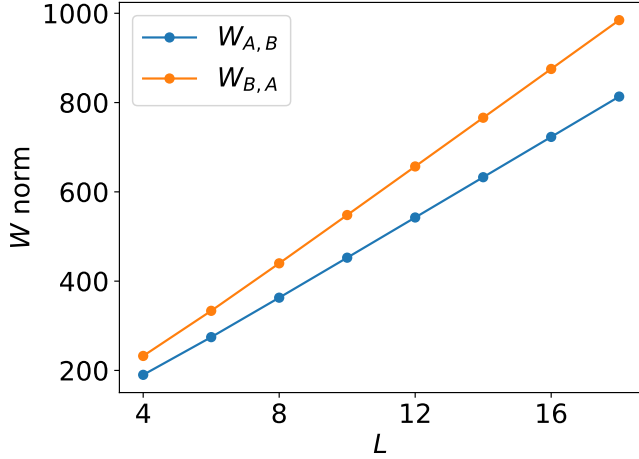


FIG. 6. System-size dependence of the W norms for the example model (28)

Note that interchanging A and B also leads to

$$\|U(\delta t) - e^{-iB\delta t/2}e^{-iA\delta t}e^{-iB\delta t/2}\| \leq W_{B,A}\delta t^3. \quad (\text{C3})$$

If $W_{A,B} < W_{B,A}$, Inequality (C1) gives a tighter bound, and one may use the second-order formula $e^{-iA\delta t/2}e^{-iB\delta t}e^{-iA\delta t/2}$ in this order of A and B . Otherwise, one may use $e^{-iB\delta t/2}e^{-iA\delta t}e^{-iB\delta t/2}$ whose error is bounded by Inequality (C3)

The W norms, $W_{A,B}$ and $W_{B,A}$, for our example model (28) discussed in the main text are plotted in Fig. 6. Recall that we focused on $e^{-iA\delta t/2}e^{-iB\delta t}e^{-iA\delta t/2}$ in the main text, and this is consistent with the tighter bound (C1) since $W_{A,B} < W_{B,A}$.

The error-bound approach based on the bound (C1) determines δt from

$$W_{A,B}\delta t^3 \leq \epsilon. \quad (\text{C4})$$

The possible maximum for δt satisfying this inequality is denoted by δt_{bound} and given in Eq. (30).

Appendix D: Comparison with Richardson's extrapolation

In this appendix, we compare Trotter24 and Richardson's extrapolation as follows. We first implement the Trotter24 like in Sec. V to obtain the magnetization expectation values at times t_N ($N = 1, 2, \dots$). On the other hand, for each time t_N , we aim to obtain a good estimate for the exact expectation value using Richardson's extrapolation. Namely, for each integer M taken out of $m + 1$ integers, we implement the usual second-order Trotterization with stepsize t_N/M , having expectation values at t_N . To equate the maximum required gate complexity in both methods, we impose $M \leq N$.

Figure 7 shows the comparison at $t = t_{10}$ and t_{40} , where Trotter24 is observable-based with $\epsilon = 10^{-2}$.

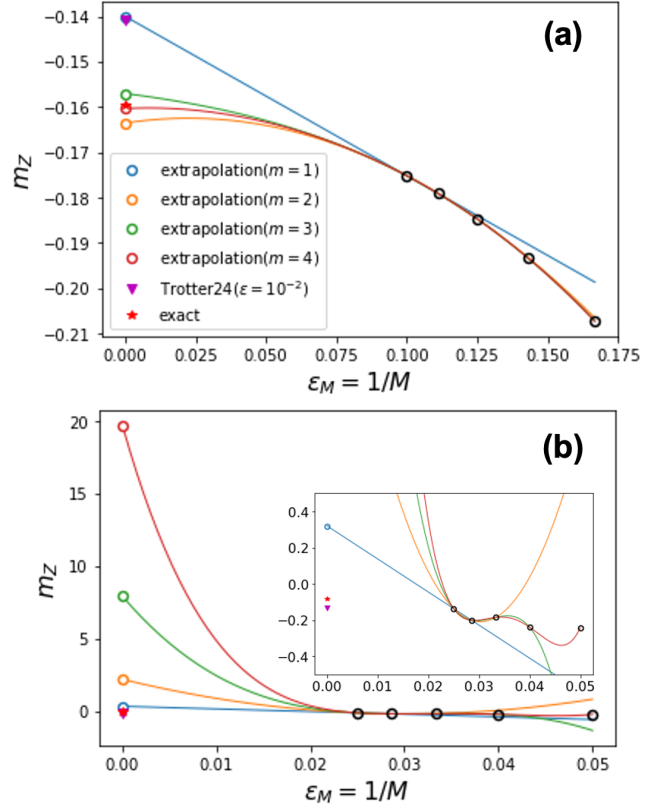


FIG. 7. Comparison between Trotter24 and Richardson's extrapolation at $t_{10} = 1.68$ (a) and $t_{40} = 10.3$ (b). Filled symbols show the magnetization expectation values obtained by the exact calculation (star) and by the observable-based Trotter24 with $\epsilon = 10^{-2}$. Open black circles show those obtained by the second-order Trotterization, m of which are polynomially extrapolated to estimate the ideal limit $\epsilon_M \rightarrow 0$ (colored circles shown in the legends).

Panel (a) shows results for the shorter $t_{10} = 1.68$. While the accuracy for $m = 1$ is comparable to Trotter24, the extrapolation gives a better estimation as m increases to outperform Trotter24. In contrast, Panel (b) shows the results for the longer $t_{40} = 10.3$, where the extrapolation gives a worse estimation as m increases.

This breakdown of extrapolations for longer times is explained by Runge's phenomenon. The expectation values of O obtained by the second-order Trotterization reads

$$O(t, \epsilon_M) = \left\langle \psi(0) \left| T_2^\dagger(\epsilon_M t)^M O T_2(\epsilon_M t)^M \right| \psi(0) \right\rangle, \quad (\text{D1})$$

where $\epsilon_M \equiv 1/M$, and we assume that $O(t, \epsilon_M)$ is $(m + 1)$ -times differentiable with respect to ϵ_M . Note that the exact value is given by $O(t, 0) = \langle \psi(0) | U(t)^\dagger O U(t) | \psi(0) \rangle = \lim_{M \rightarrow \infty} O(t, \epsilon_M)$. The extrapolation method estimates this by extrapolating an m -th order polynomial curve going through the $(m + 1)$ points, $(\epsilon_{M_0}, O(t, \epsilon_{M_0})), \dots, (\epsilon_{M_m}, O(t, \epsilon_{M_m}))$, where we assume $M_0 > \dots > M_m$. Thus, utilizing the coefficients

c_i obtained through Neville's algorithm, we can write the estimate as $\tilde{O}_m(t, 0) = \sum_{i=0}^m c_i O(t, \varepsilon_{M_i})$. Then, the error

of the estimate is bounded as

$$|O(t, 0) - \tilde{O}_m(t, 0)| \leq \max_{0 \leq \xi \leq \varepsilon_{M_m}} \frac{1}{(m+1)!} \left| \frac{\partial^{(m+1)} O(t, \xi)}{\partial \varepsilon_M^{(m+1)}} \right| \prod_{i=0}^m \varepsilon_{M_i}. \quad (\text{D2})$$

Notice that $\max_{0 \leq \xi \leq \varepsilon_{M_m}} \left| \frac{\partial^{(m+1)} O(t, \xi)}{\partial \varepsilon_M^{(m+1)}} \right|$ can increase when m increases. Consequently, the extrapolation estimates can be worse even though we increase m , and this is known as Runge's phenomenon. This phenomenon can occur when m is too large even if t is short. Generally speaking, $O(t, \varepsilon_M)$ tends to become a more complex function of ε_M as t increases, leading to instability.

Runge's phenomenon is circumvented, in classical numerics, by optimizing the sequence $\varepsilon_0, \varepsilon_1, \dots, \varepsilon_m$ such as the Chebyshev nodes. However, this type of optimization is nontrivial in NISQ devices because of the limitation of circuit depth and the constraint that M_i 's are integers. In fact, a recent study [37] resorts to a beyond-NISQ quantum computation for solving the optimization. Trotter24 is free from Runge's phenomenon and more stable especially in longer times.

-
- [1] A. W. Harrow and A. Montanaro, Quantum computational supremacy, *Nature* **549**, 203 (2017).
- [2] Y. Cao, J. Romero, J. P. Olson, M. Degroote, P. D. Johnson, M. Kieferová, I. D. Kivlichan, T. Menke, B. Peropadre, N. P. D. Sawaya, S. Sim, L. Veis, and A. Aspuru-Guzik, Quantum chemistry in the age of quantum computing, *Chemical Reviews* **119**, 10856 (2019).
- [3] M. Cerezo, A. Arrasmith, R. Babbush, S. C. Benjamin, S. Endo, K. Fujii, J. R. McClean, K. Mitarai, X. Yuan, L. Cincio, and P. J. Coles, Variational quantum algorithms, *Nature Reviews Physics* **3**, 625 (2021).
- [4] A. Aspuru-Guzik, A. D. Dutoi, P. J. Love, and M. Head-Gordon, Simulated quantum computation of molecular energies, *Science* **309**, 1704 (2005).
- [5] S. Lloyd, Universal quantum simulators, *Science* **273**, 1073 (1996).
- [6] J. D. Whitfield, J. Biamonte, and A. Aspuru-Guzik, Simulation of electronic structure hamiltonians using quantum computers, *Molecular Physics* **109**, 735 (2011), <https://doi.org/10.1080/00268976.2011.552441>.
- [7] O. Higgott, D. Wang, and S. Brierley, Variational Quantum Computation of Excited States, *Quantum* **3**, 156 (2019).
- [8] T. Jones, S. Endo, S. McArdle, X. Yuan, and S. C. Benjamin, Variational quantum algorithms for discovering hamiltonian spectra, *Phys. Rev. A* **99**, 062304 (2019).
- [9] W. M. Kirby and P. J. Love, Variational quantum eigensolvers for sparse hamiltonians, *Phys. Rev. Lett.* **127**, 110503 (2021).
- [10] R. Babbush, J. McClean, D. Wecker, A. Aspuru-Guzik, and N. Wiebe, Chemical basis of trotter-suzuki errors in quantum chemistry simulation, *Phys. Rev. A* **91**, 022311 (2015).
- [11] G. H. Low and I. L. Chuang, Optimal hamiltonian simulation by quantum signal processing, *Phys. Rev. Lett.* **118**, 010501 (2017).
- [12] E. Campbell, Random compiler for fast hamiltonian simulation, *Phys. Rev. Lett.* **123**, 070503 (2019).
- [13] D. An, D. Fang, and L. Lin, Time-dependent unbounded Hamiltonian simulation with vector norm scaling, *Quantum* **5**, 459 (2021).
- [14] D. An, D. Fang, and L. Lin, Time-dependent Hamiltonian Simulation of Highly Oscillatory Dynamics and Superconvergence for Schrödinger Equation, *Quantum* **6**, 690 (2022).
- [15] A. M. Childs, J. Leng, T. Li, J.-P. Liu, and C. Zhang, Quantum simulation of real-space dynamics, *Quantum* **6**, 860 (2022).
- [16] B. Swingle, G. Bentsen, M. Schleier-Smith, and P. Hayden, Measuring the scrambling of quantum information, *Phys. Rev. A* **94**, 040302 (2016).
- [17] J. Zhang, P. W. Hess, A. Kyprianidis, P. Becker, A. Lee, J. Smith, G. Pagano, I.-D. Potirniche, A. C. Potter, A. Vishwanath, N. Y. Yao, and C. Monroe, Observation of a discrete time crystal, *Nature* **543**, 217 (2017).
- [18] K. A. Landsman, C. Figgatt, T. Schuster, N. M. Linke, B. Yoshida, N. Y. Yao, and C. Monroe, Verified quantum information scrambling, *Nature* **567**, 61 (2019).
- [19] L. K. Joshi, A. Elben, A. Vikram, B. Vermersch, V. Galitski, and P. Zoller, Probing many-body quantum chaos with quantum simulators, *Phys. Rev. X* **12**, 011018 (2022).
- [20] A. Y. Kitaev, Quantum measurements and the abelian stabilizer problem (1995), [arXiv:quant-ph/9511026](https://arxiv.org/abs/quant-ph/9511026).
- [21] H. F. Trotter, On the Product of Semi-Groups of Operators, *Proceedings of the American Mathematical Society* **10**, 545 (1959).
- [22] N. Hatano and M. Suzuki, Finding Exponential Product Formulas of Higher Orders, in *Quantum Annealing and Other Optimization Methods*, edited by A. Das and B. K. Chakrabarti (Springer Berlin Heidelberg, Berlin, Heidelberg, 2005) pp. 37–68.
- [23] J. Preskill, Quantum Computing in the NISQ era and beyond, *Quantum* **2**, 79 (2018).
- [24] Y. Kim, A. Eddins, S. Anand, K. X. Wei, E. van den Berg, S. Rosenblatt, H. Nayfeh, Y. Wu, M. Zaletel,

- K. Temme, and A. Kandala, Evidence for the utility of quantum computing before fault tolerance, *Nature* **618**, 500 (2023).
- [25] I. D. Kivlichan, C. Gidney, D. W. Berry, N. Wiebe, J. McClean, W. Sun, Z. Jiang, N. Rubin, A. Fowler, A. Aspuru-Guzik, H. Neven, and R. Babbush, Improved Fault-Tolerant Quantum Simulation of Condensed-Phase Correlated Electrons via Trotterization, *Quantum* **4**, 296 (2020).
- [26] A. M. Childs, Y. Su, M. C. Tran, N. Wiebe, and S. Zhu, Theory of trotter error with commutator scaling, *Phys. Rev. X* **11**, 011020 (2021).
- [27] Q. Zhao, Y. Zhou, A. F. Shaw, T. Li, and A. M. Childs, Hamiltonian simulation with random inputs, *Phys. Rev. Lett.* **129**, 270502 (2022).
- [28] H. Zhao, M. Bukov, M. Heyl, and R. Moessner, Making trotterization adaptive for NISQ devices and beyond, (2022), [arXiv:2209.12653 \[quant-ph\]](https://arxiv.org/abs/2209.12653).
- [29] After the submission of our work, Zhao et al. [42] publicized their adaptive-stepsize Trotterization generalized to time-dependent Hamiltonians.
- [30] E. Forest and R. D. Ruth, Fourth-order symplectic integration, *Physica D: Nonlinear Phenomena* **43**, 105 (1990).
- [31] M. Suzuki, Fractal decomposition of exponential operators with applications to many-body theories and Monte Carlo simulations, *Physics Letters A* **146**, 319 (1990).
- [32] I. P. Omelyan, I. M. Mryglod, and R. Folk, Optimized Forest–Ruth- and Suzuki-like algorithms for integration of motion in many-body systems, *Computer Physics Communications* **146**, 188 (2002).
- [33] J. Ostmeier, Optimised trotter decompositions for classical and quantum computing, *Journal of Physics A: Mathematical and Theoretical* **56**, 285303 (2023).
- [34] R. D. Ruth, A canonical integration technique, *IEEE Trans. Nucl. Sci.* **30**, 2669 (1983).
- [35] S. Endo, S. C. Benjamin, and Y. Li, Practical quantum error mitigation for near-future applications, *Phys. Rev. X* **8**, 031027 (2018).
- [36] S. Endo, Q. Zhao, Y. Li, S. Benjamin, and X. Yuan, Mitigating algorithmic errors in a hamiltonian simulation, *Phys. Rev. A* **99**, 012334 (2019).
- [37] G. Rendon, J. Watkins, and N. Wiebe, Improved error scaling for trotter simulations through extrapolation, [arXiv preprint arXiv:2212.14144](https://arxiv.org/abs/2212.14144) (2022).
- [38] T. N. Ikeda, A. Abrar, I. L. Chuang, and S. Sugiura, Minimum Trotterization Formulas for a Time-Dependent Hamiltonian, *Quantum* **7**, 1168 (2023).
- [39] G. Vidal, Efficient simulation of one-dimensional quantum many-body systems, *Phys. Rev. Lett.* **93**, 040502 (2004).
- [40] Z. Cai, R. Babbush, S. C. Benjamin, S. Endo, W. J. Huggins, Y. Li, J. R. McClean, and T. E. O’Brien, Quantum error mitigation (2022), [arXiv:2210.00921](https://arxiv.org/abs/2210.00921).
- [41] Y. Suzuki, Y. Kawase, Y. Masumura, Y. Hiraga, M. Nakadai, J. Chen, K. M. Nakanishi, K. Mitarai, R. Imai, S. Tamiya, T. Yamamoto, T. Yan, T. Kawakubo, Y. O. Nakagawa, Y. Ibe, Y. Zhang, H. Yamashita, H. Yoshimura, A. Hayashi, and K. Fujii, Qulacs: a fast and versatile quantum circuit simulator for research purpose, *Quantum* **5**, 559 (2021).
- [42] H. Zhao, M. Bukov, M. Heyl, and R. Moessner, Adaptive trotterization for time-dependent hamiltonian quantum dynamics using instantaneous conservation laws (2023), [arXiv:2307.10327](https://arxiv.org/abs/2307.10327).